



Tetherless near-infrared control of brain activity in behaving animals using fully implantable upconversion microdevices



Ying Wang^{a,1}, Xudong Lin^{a,1}, Xi Chen^{b,1}, Xian Chen^c, Zhen Xu^a, Wenchong Zhang^a, Qinghai Liao^d, Xin Duan^b, Xin Wang^b, Ming Liu^d, Feng Wang^c, Jufang He^b, Peng Shi^{a,e,*}

^a Department of Mechanical and Biomedical Engineering, City University of Hong Kong, Kowloon, 999077, Hong Kong, China

^b Department of Biomedical Science, City University of Hong Kong, Kowloon, 999077, Hong Kong, China

^c Department of Physics and Material Science, City University of Hong Kong, Kowloon, 999077, Hong Kong, China

^d Robotics and Multi-perception Lab, Department of Electronic and Computer Engineering, Hong Kong University of Science and Technology, Kowloon, 999077, Hong Kong, China

^e Shenzhen Research Institute, City University of Hong Kong, Shenzhen, 518000, China

ARTICLE INFO

Article history:

Received 29 June 2017

Received in revised form

7 July 2017

Accepted 9 July 2017

Available online 12 July 2017

Keywords:

Upconversion materials

Neural stimulation

Near-infrared light

Remote control

Wireless optogenetics

ABSTRACT

Many nanomaterials can be used as sensors or transducers in biomedical research and they form the essential components of transformative novel biotechnologies. In this study, we present an all-optical method for tetherless remote control of neural activity using fully implantable micro-devices based on upconversion technology. Upconversion nanoparticles (UCNPs) were used as transducers to convert near-infrared (NIR) energy to visible light in order to stimulate neurons expressing different opsin proteins. In our setup, UCNPs were packaged in a glass micro-optrode to form an implantable device with superb long-term biocompatibility. We showed that remotely applied NIR illumination is able to reliably trigger spiking activity in rat brains. In combination with a robotic laser projection system, the upconversion-based tetherless neural stimulation technique was implemented to modulate brain activity in various regions, including the striatum, ventral tegmental area, and visual cortex. Using this system, we were able to achieve behavioral conditioning in freely moving animals. Notably, our microscale device was at least one order of magnitude smaller in size (~100 μm in diameter) and two orders of magnitude lighter in weight (less than 1 mg) than existing wireless optogenetic devices based on light-emitting diodes. This feature allows simultaneous implantation of multiple UCNP-optrodes to achieve modulation of brain function to control complex animal behavior. We believe that this technology not only represents a novel practical application of upconversion nanomaterials, but also opens up new possibilities for remote control of neural activity in the brains of behaving animals.

© 2017 Elsevier Ltd. All rights reserved.

1. Introduction

Electrical, optical, and chemical manipulations of neural circuits have been major approaches used to elucidate the functions and connections of the nervous system. Recently, optogenetics has become a versatile and transformative tool for neuroscience studies [1,2]. The technique is based on optical stimulation of light-sensitive ion channels genetically expressed on cell membranes, and thus allows for spatially and temporally precise control over neural activity

* Corresponding author. Department of Mechanical and Biomedical Engineering, City University of Hong Kong, Kowloon, 999077, Hong Kong, China.

E-mail address: pengshi@cityu.edu.hk (P. Shi).

¹ These authors contributed equally to this work.

[3–5]. Since the first demonstration using channelrhodopsin-2 (ChR2), various photosensitive proteins have been developed to provide flexible options for optogenetic applications [6–9]. Most of these proteins are activated by light within the visible spectrum (VIS), which has limited tissue penetration and can lead to great photo-toxicity following prolonged exposure [10]. A typical optogenetic experiment usually requires light delivery by implanted optic fibers connected to a light source [11]. In many behavioral tests, such tethered systems prevent animals from moving freely and impose significant constraints on experimental design. These systems also complicate the analysis of animal behavior. Recently, great efforts have been made to develop tether-free optogenetic strategies [12–15]. Many of these techniques utilize wirelessly powered light-

emitting diodes (LEDs) to deliver visible light for optogenetic stimulation of deep brain regions. Even though implantable LED devices and associated powering circuits have become smaller, lighter, and more versatile [12,15], the requirement for electronic components still complicates the fabrication and implementation procedures. Thus, a simple, all-optical, tetherless optogenetic method remains attractive and is yet to be developed.

Conceptually, light in the near-infrared (NIR, 700–1100 nm) range would be a preferable source for tether-free optogenetic applications, given its advantages, which include deep tissue penetration, low absorbance by biomolecules, and minimal photo-induced damage to mammalian cells [16]. However, direct excitation of ChR proteins at wavelengths in the NIR spectrum is challenging despite tremendous efforts in the development of red-shifted ChR variants through intricate protein engineering [6,8,17]. Two-photon fluorescence microscopy (TPFM) has been adopted for optogenetic analysis of neural circuitry using NIR to stimulate specific ChR variants [18–21]. However, TPFM-based optogenetics techniques are limited by drawbacks, such as small illumination volume, complex optical setup, and low compatibility with *in vivo* experiments, especially in freely moving animals [22,23]. Alternatively, transducing elements, such as upconversion nanoparticles (UCNPs), can be used to bridge the spectral gap between NIR and VIS. Upon excitation by lower-energy NIR photons, UCNPs can reliably emit shorter wavelengths within the VIS spectrum [24]. Recently, UCNPs have been used in different *in vivo* applications, such as non-invasive imaging of deep tissues, drug delivery, and photodynamic therapy [25–27]. When combined with different opsin proteins, UCNP techniques may have unique potential as novel and straightforward methods to achieve tetherless optogenetic control in deep brain regions [28,29].

In this study, we demonstrated all-optical tetherless brain stimulation using upconversion based NIR-actuated micro-devices. NaYF₄-based nanoparticles were used as optical transducers to convert NIR energy to visible light used to stimulate neurons expressing opsin proteins. The fully implantable microscale device was based on a UCNP-embedded glass micro-optrode, which was excited by an NIR laser (980 nm) to emit green or blue light, depending on different dopants in the nanoparticles. When the optrodes were implanted into the brain infected to express ChR2 or C1V1, NIR illumination reliably stimulated the neurons to fire action potentials. The upconversion-based device was then integrated with robotic instrumentation to implement an all-optical tetherless neural stimulation strategy. To demonstrate the unique advantages of the system for behavioral experiments in live animals, the UCNP-optrodes were implanted at various locations in mouse or rat brains. These locations included the cortical striatum, ventral tegmental area (VTA), and visual cortex. Our technique was successfully utilized to condition motor or learning behavior in freely moving animals. Because of the microscale size (~100 μm in diameter) and extremely light weight (less than 1 mg) of the UCNP-based implants, multiple devices could be simultaneously placed in a rodent brain to achieve sufficient activation to modulate complex brain function. We also demonstrated the long-term biocompatibility and functionality of the UCNP-optrode device, which remained effective even six months after surgical implantation. In sum, the upconversion-based tetherless neural stimulation technology opens up new possibilities and creates flexibility for remote control in deep brain regions, and can be easily adopted by other laboratories.

2. Results

2.1. System design

The emission of visible light from upconversion results from

sequential discrete absorption of two or more lower-energy photons. Though this process can potentially enable the implementation of a method using NIR to stimulate neurons expressing commonly used light-sensitive ion channel proteins (e.g., ChR and C1V1, Fig. 1a), several technical challenges must be overcome before any practical implementation. First, the UCNPs need to be implanted in a biocompatible format with sufficient concentration, so that the implants are not toxic and the upconversion emission is sufficient to evoke optogenetic response. Second, the NIR irradiation has to target a specific part of the body of the freely moving animal (e.g., head for brain stimulation) for consistent tetherless delivery of stimulus signals. Accordingly, we made a fully implantable transducer device by sealing dry UCNPs in a glass micro-pipette to form an optrode (Fig. 1b and c). This package guarantees that there is no direct contact between the nanoparticles and neurons, effectively providing the UCNP-optrode with the same biocompatibility as an optical fiber, which is widely used in traditional optogenetic experiments. The micro-device was only ~100 μm in diameter and less than 1 mg in weight, which is greatly beneficial in preserving tissue integrity, as it leads to negligible brain lesion during surgical implantation. For remote delivery of NIR to the targeted body part of a behaving rodent (Fig. 1d), we further designed a robotic laser projection system, which was capable of automatically tracing the animal's head. We were able to place a single NIR illumination spot (3 cm in diameter) on the head of the rodent in real-time so that consistent NIR stimulation could be achieved (Fig. 1e). In this system, two rotational motors and a 3D-printed holding adaptor were assembled to form a robotic arm, which was placed ~50 cm above the arena and was used to project NIR illumination at arbitrary coordinates in a 40 × 40 cm experimental field. The control of the robotic arm and subsequently the placement of illumination spot were achieved using a custom image recognition program. The implantable UCNP-optrode and the autonomous laser projection system thus form a novel all-optical solution for tetherless control of brain function in freely moving animals.

2.2. Characterization of the upconversion-based transducer device

Engineered core-shell nanoparticles were used to make the UCNP transducer device (Fig. 2a). The nanostructure produces unique optical properties that are inaccessible by its bulkier counterparts [30]. UCNPs composed of lanthanide-doped NaYF₄ were fabricated via a layer-by-layer growth process and used as light transducers in this study. Our sophisticated nano-synthesis protocol offered exquisite control over particle size, morphology, and doping strategy with high reproducibility. The uniform spherical shape of the core, which had an average size of ~20 nm, was seen in transmission electron microscopy images in Fig. 2b. The particle size was slightly increased with some morphological variation in the corresponding core-shell UCNPs used in this study (Fig. 2c). Upon NIR (980 nm) illumination, the UCNPs comprising Tm³⁺ (or Er³⁺) dopants in the core emitted blue (or green) light peaking at 470 nm (or 540 nm). After being packaged in a micro-optrode, the device typically produced an upconversion efficiency of ~4%, and the emission power of blue or green light was positively correlated with the input NIR power (Fig. 2d and e). Though this efficiency is relatively low, the intensity of visible light emission could be sufficient for regular optogenetic stimulation, which has a power density requirement of 1–5 mW/mm² [1].

2.3. Sufficient tissue penetration under safe NIR irradiation

As NIR energy is not strongly absorbed by water or biomolecules, NIR can penetrate much deeper into tissue than visible light [16], which is highly phototoxic and may cause serious damage

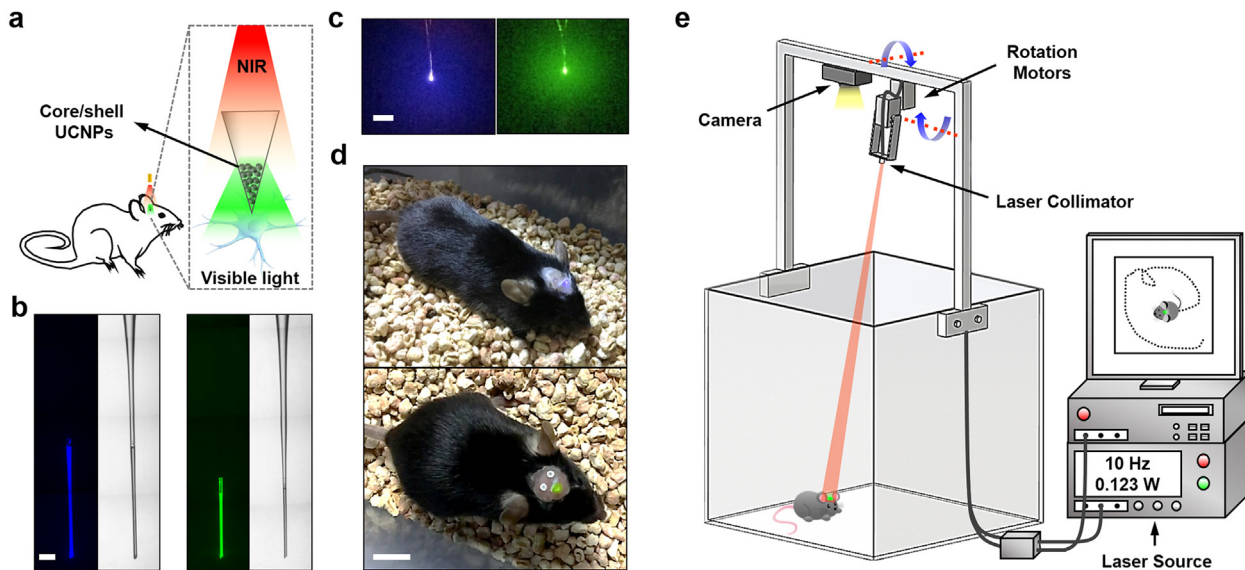


Fig. 1. Upconversion-based neural stimulation technique. (a) Schematic of tetherless near-infrared (NIR) optogenetic control of brain activity using fully implantable upconversion microdevices. (b) Bright-field and fluorescent photographs of the implantable micro-optrodes containing upconversion nanoparticles (UCNPs) doped with Tm^{3+} (blue) or Er^{3+} (green). Scale bar, 500 μm . (c) Fluorescent images of the operating UCNP micro-devices (Tm^{3+} -doped, blue; Er^{3+} -doped, green) excited by NIR. Scale bar, 2 mm. (d) Images of animals implanted with different types of micro-optrodes containing Tm^{3+} -doped (top) or Er^{3+} -doped (bottom) UCNPs. Scale bar, 1 cm. (e) Instrumentation design of a robotic laser projection system for automatic and consistent NIR irradiation of the heads of behaving animals. (For interpretation of the references to colour in this figure legend, the reader is referred to the web version of this article.)

to human and animal eyes. NIR lasers are much less hazardous and safer to operate, as the major potential damage by NIR irradiation consists of the induced thermal effect. We next evaluated the thermal effects of NIR at an illumination power ($8 \text{ mW}/\text{mm}^2$) much higher than the typical experimental settings required to drive UCNP-optrodes. We used infrared imaging to monitor the temperature change of the sample in real time, and showed that pulsed illumination of the 980 nm laser induced almost no temperature change on the skin of the animal (Fig. 3a and b). Furthermore, using an isolated rat brain, we showed that upconversion emission does not lead to any heating effects at the tip of the micro-optrode, even though UCNPs were packaged there in a highly concentrated format (Fig. 3c–e). Of note, the UCNP-optrode could still be activated to produce upconverted emission using safe NIR illumination, even after being inserted through a whole rat brain ($\sim 1 \text{ cm}$ thick, Fig. 3c, Supplementary Movie S1). This penetration depth is sufficient to accommodate all experiments involving neural stimulation in various brain structures. In the following experiments, our power settings for NIR irradiation were well below the conservative limits established for human skin exposure to 980 nm light ($7.26 \text{ mW}/\text{mm}^2$) [31].

Supplementary video related to this article can be found at <http://dx.doi.org/10.1016/j.biomaterials.2017.07.017>.

2.4. Remote regulation of electrophysiological activity in rat brains

To demonstrate effective neuronal stimulation by the NIR-actuated upconversion process, we implanted the UCNP-optrode in the brain of a living animal to stimulate ChR2- or C1V1-expressing neurons, which were characterized by *in vivo* electrophysiology recordings (Fig. 4a). Micro-optrodes containing Tm^{3+} or Er^{3+} -doped UCNPs were implanted into the virus injection site along with tungsten electrodes ($1.2 \text{ M}\Omega$ impedance, Supplementary Fig. S1a). When the 980 nm laser (40 ms, 0.2 Hz, $7 \text{ mW}/\text{mm}^2$ for ChR2; or 40 ms, 0.2 Hz, $4.4 \text{ mW}/\text{mm}^2$ for C1V1) was applied, visible light from the UCNP-optrode reliably induced neuronal spiking

activity at the corresponding time points. Similar activation was not observed in virus-infected animals implanted with a null-optrode (Fig. 4b). The temporal correlation between NIR illumination and evoked neuronal spiking was further confirmed using peri-stimulus time histograms (PSTHs) from representative electrodes (Fig. 4c and d). These results proved the basic feasibility of upconversion-based NIR-optogenetics for controlling neural activity in brains of live animals without the need for in-tissue light delivery by tethered fiber optics.

2.5. Tetherless transcranial brain stimulation in behaving mice

In combination with the robotic laser projection device as described above (Fig. 1a), we next implemented an all-optical tetherless system to test the effectiveness of the upconversion-based neural stimulation strategy, and see if it can be used for behavioral conditioning in freely moving mice (Fig. 5a). In this demonstration, a micro-optrode containing Er^{3+} -doped UCNPs was implanted in the cortical striatum (stereotaxic coordinates: 1.1 mm posterior, 1.7 mm lateral, 3 mm ventral) of C1V1-infected mice for unilateral stimulation upon NIR illumination (Fig. 5b). The surgery site was fully covered by dental cement, which was further screwed to the surrounding skull to ensure long-term stability of the implants (Supplementary Fig. S1b–f). The animals were individually placed in open experimental fields defined by a cylinder 30 cm in diameter and NIR illumination (10 ms pulse width, 20 Hz, $5 \text{ mW}/\text{mm}^2$) was consistently applied to their heads (Supplementary Movie S2). The animals' movements were simultaneously monitored by video-tracking (Supplementary Fig. S2). We showed that NIR could dramatically change the locomotion patterns of C1V1 mice following unilateral stimulation of the cortical striatum (Fig. 5c). We induced significantly more contraversive turning in these animals than in control groups [32,33] ($4.68 \pm 0.26/\text{min}$. vs. $1.48 \pm 0.17/\text{min}$., mean \pm s.e.m., Fig. 5d and Supplementary Movie S3). Furthermore, the UCNP-device was functional even after 6 months in the mouse brain (Fig. 5d), suggesting the utility of this

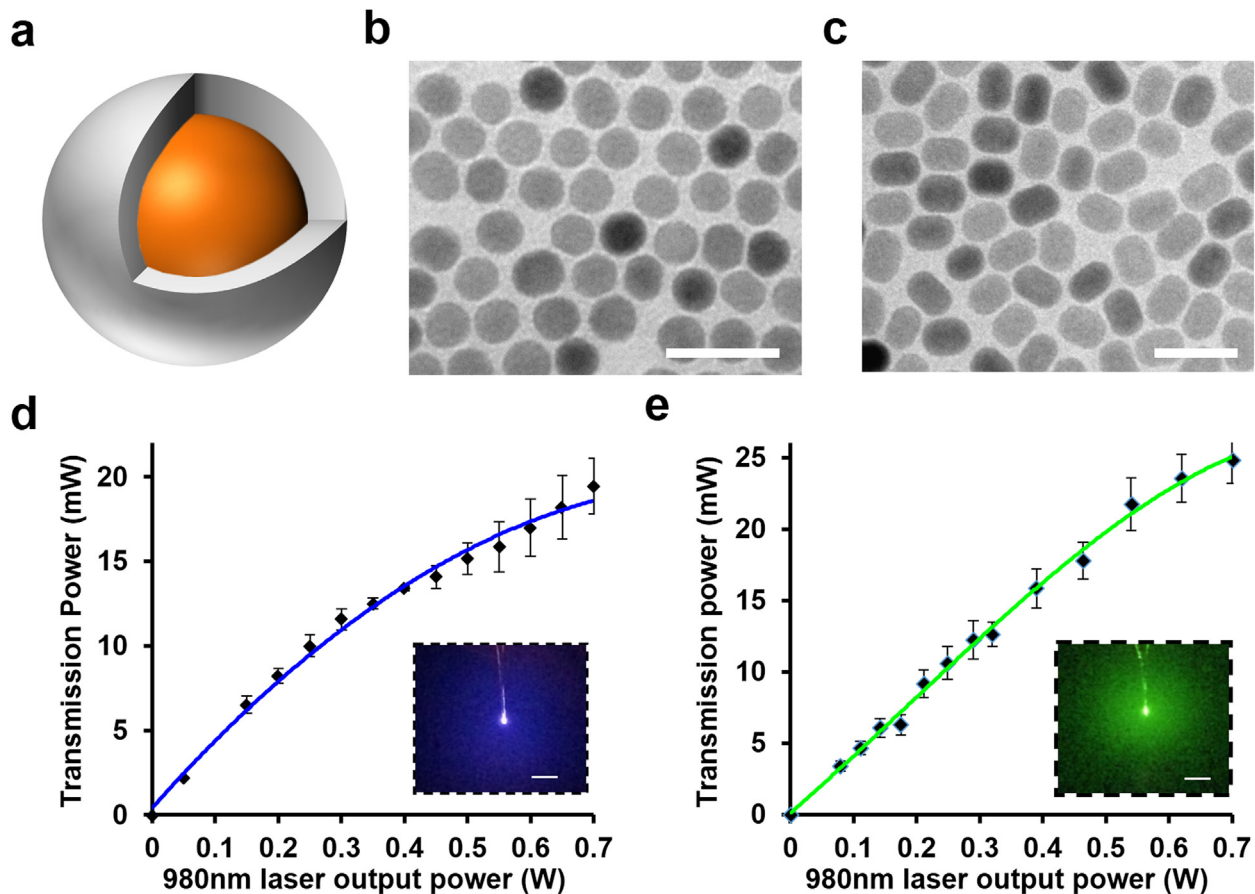


Fig. 2. Physical characterization of the upconversion-based transducer device. (a) Schematic of the core-shell structure of UCNPs (not to scale). (b) Transmission electron microscopy (TEM) images of the NaYF₄:Yb/Er core. Scale bar, 100 nm. (c) TEM image of the NaYF₄:Yb/Er@NaYF₄ core-shell nanoparticles. Scale bar, 100 nm. (d) The power of blue light emission from micro-optrodes containing UCNPs doped with Tm³⁺ at various powers of the 980 nm laser. Scale bar, 2 mm. (e) The power of green light emission from micro-optrodes containing UCNPs doped with Er³⁺ at various powers of the 980 nm laser. Scale bar, 2 mm. (For interpretation of the references to colour in this figure legend, the reader is referred to the web version of this article.)

technique in long-term chronic experiments. For the first time, our integration of upconversion technology and robotic instrumentation clearly demonstrated an all-optical solution for flexible tetherless control of brain activity.

Supplementary video related to this article can be found at <http://dx.doi.org/10.1016/j.biomaterials.2017.07.017>.

2.6. Deep brain stimulation

To show its utility for deep brain stimulation, the upconversion-based tetherless neural modulation method was further tested to stimulate the VTA (~4.5 mm deep) in mice. We used the device to control dopamine reward behavior in these animals while they explored a complex environment in a Y-shaped maze (Fig. 6a). As previously reported, phasic firing of dopaminergic neurons in the VTA is sufficient for behavioral conditioning [34]. We transduced VTA tissue to express C1V1 and examined whether NIR illumination could engage the animals in a location-oriented self-stimulation dopamine reward pathway. As shown in Fig. 6b, many dopamine neurons (positive for tyrosine hydroxylase, TH⁺) co-expressed C1V1 in the VTA region. Though it is possible that neurons in adjacent regions might also be infected to express ChR proteins due to the non-specific nature of the CaMKII promoter, proper stimulation of the VTA was further ensured by the precise placement of the microscale UCNP-optrode using a stereotaxic apparatus. In this experiment, mice were allowed to explore a Y-maze with three arms, each of which was equipped with a custom-

made nose-poking apparatus at the distal end (Supplementary Fig. S3). Nose-poking at one specific arm (“Active”) was paired with 980 nm illumination (10 pulses, 20 Hz, 10 ms width, 5 mW/mm²). As shown in Fig. 6c–g, C1V1 mice learned to self-stimulate their dopamine neurons by selectively approaching and poking in the “Active” arm, which triggered NIR illumination and effectively activated their VTA regions (Supplementary Movie S4). After a five-day conditioning period, around 60% of the total nose-pokes were made in the “Active” arm (Fig. 6c). This was accompanied by a significant drop in nose-pokes in the “inactive” arms (Fig. 6d). Accordingly, the mice also developed robust location preference to the “Active” arm, wherein they showed significantly higher appearance probability (59 ± 3.5%, mean ± s.e.m., n = 5) than in the other two “inactive” arms, even in the post-conditioning period, which was devoid of further NIR illumination (Fig. 6e and f). Animals receiving proper stimulation of the VTA had much more predictable movements after the NIR conditioning period, as indicated by a significant drop in the preference index (defined by information entropy of mouse appearance probabilities in all three arms, Fig. 6g). We also observed that repeated NIR irradiation for one hour (5 mW/mm², 20 Hz, 10 ms width, 10 pulses were applied at the beginning of every minute) could induce strong expression of c-fos, which is a typical biochemical marker for neuronal activation, in C1V1⁺/TH⁺ dopamine neurons surrounding the UCNP-optrode (Fig. 6h). About 76 ± 2.3% (mean ± s.e.m., n = 5) of C1V1⁺ cells within 200 μm of the optrode were activated by UCNP to express c-fos. In these chronic experiments, which lasted for more than one

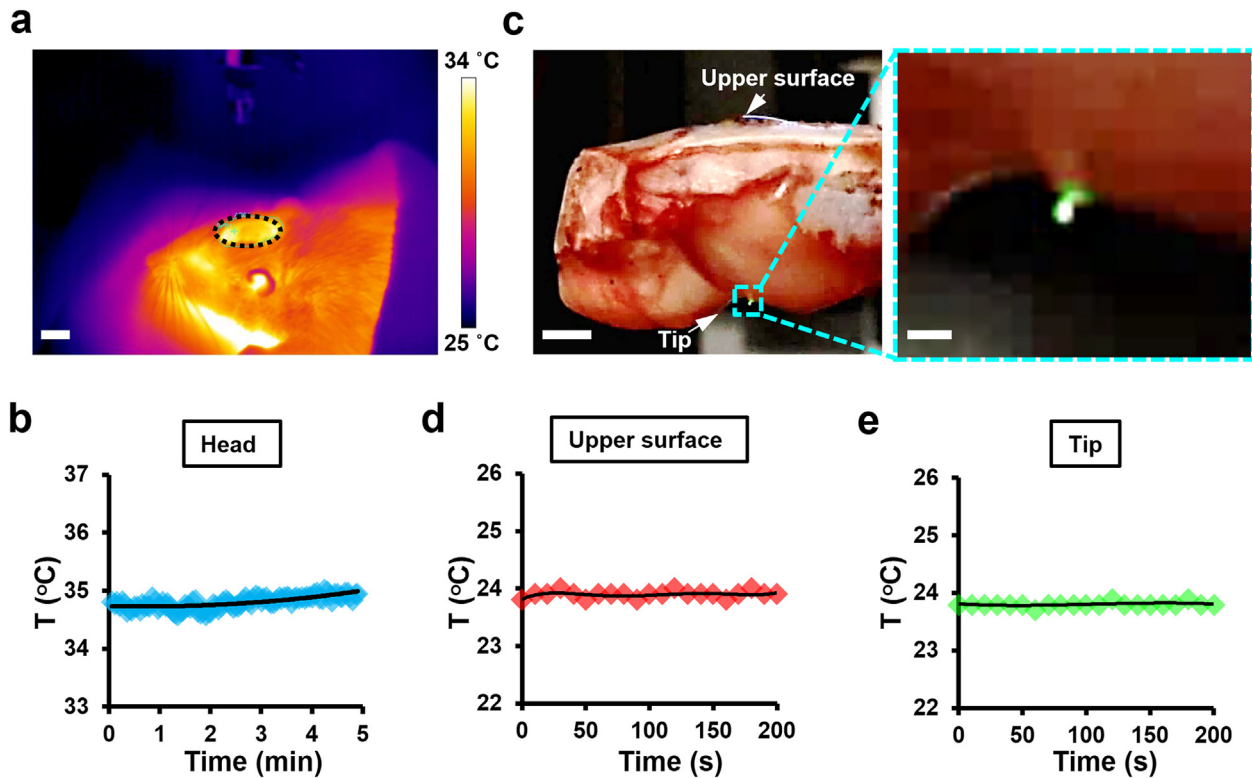


Fig. 3. Thermal characterization of NIR irradiation used to actuate upconversion-based implants. (a) Infrared imaging of a live rat's brain under pulsed NIR laser irradiation. Scale bar, 5 mm. (b) The temperature fluctuation at the center point of the NIR-irradiated region circled in panel (a). To obtain the images in panels (a) and (b), the rat's head was exposed to a pulsed 980 nm laser (50 ms width, 10 pulses, 10 Hz, 8 mW/mm²) for 5 min. (c) Evaluation of temperature fluctuation at the tip of a UCNP-optrode after implantation through an isolated rat brain. Scale bar, 2.5 mm. The boxed region is enlarged to show the green emission from the UCNP-optrode tip, which was remotely actuated by NIR irradiation above the skull. Scale bar, 500 μ m. (d) The temperature fluctuation at the upper surface of the rat's head. (e) The temperature fluctuation at the tip of the UCNP-optrode. To obtain the data shown in panels (c) and (d), the isolated rat's head was exposed to a pulsed 980 nm laser (50 ms width, 10 pulses, 10 Hz, 8 mW/mm²) over 200 s. (For interpretation of the references to colour in this figure legend, the reader is referred to the web version of this article.)

month, the fully implantable device was well-tolerated by the host brain. Only a small amount of glial activation surrounding the optrode was observed due to minor surgical lesions, and there was no significant increases in the inflammatory response, as indicated by immunostaining of activated microglia [35] (Supplementary Fig. S4). These results further established the utility and versatility of the tetherless system for controlling neural activity in deep brain regions. Our findings also highlight its compatibility with vulnerable mouse models.

Supplementary video related to this article can be found at <http://dx.doi.org/10.1016/j.biomaterials.2017.07.017>.

2.7. Implantation of multiple UCNP-optrodes

One of the advantages of the all-optical upconversion-based technique is the microscale size (\sim 100 μ m in diameter) and extremely light weight (less than 1 mg) of the implantable device. These characteristics enable multiple UCNP-optrodes to be simultaneously implanted to achieve complex manipulation of brain function (Fig. 7a–c). As demonstrated here, an array of four UCNP-optrodes were implanted into the visual cortex of ChR2 rats to ensure sufficient activation. We used the device to pair water-seeking activity in a two-port operant chamber with neural stimulation in cortical tissue, which was controlled by a brief NIR exposure (Fig. 7c). The co-localization of the implanted UCNP-optrodes and the ChR2-expressing region was directly validated using a multimodal animal imaging system with X-Ray and fluorescent capabilities (Fig. 7d). When an animal was placed in the dual-port chamber, it was required to insert its nose into the left

port to initiate a trial after a variable holding period (800–1500 ms). A stimulus consisting of 10 NIR pulses (980 nm, 10 Hz, 50 ms pulse width, 1.5 mW/mm²) was remotely applied over the animal's head. The activation of the visual cortex subsequently cued the animal to obtain a water reward from the right port (Fig. 7c). Successfully stimulated rats gradually responded to NIR signals after being trained for 3–4 days. These rats were triggered to obtain water rewards in a well-controlled pattern immediately after every NIR illumination cycle (Supplementary Movie S5). Their performance was evaluated by either reaction time or success rate in obtaining rewards from the right port. On the 4th training day, the reaction times following the onset of the 980 nm laser were significantly reduced in properly stimulated subjects (Fig. 7e, $p < 0.001$, paired Kruskal-Wallis test, $n = 4$, at least 200 trials for each subject) when compared to animals in different control groups. As an animal's performance may depend on their expectation about the occurrence moment of the NIR cue, we intentionally randomized the switching on of the NIR cue using a varying holding period (800–1500 ms) after a nose-poke in the left port to prevent rats from predicting the stimulus. The reaction times were mostly between \sim 100 to \sim 400 ms in the ChR2 animals, and were significantly different when compared to the results obtained from animals in control groups, which had much more even distributions of reaction times during the period between 0 and 1500 ms (Fig. 7f). Accordingly, a successfully triggered trial was defined as a rewarded movement within a temporal window of 100–600 ms from the onset of NIR. After 4 days of training, the success rates of the NIR-triggered tasks gradually increased from \sim 50% to almost \sim 80% in the UCNP-optrode-implanted animals receiving 980 nm laser

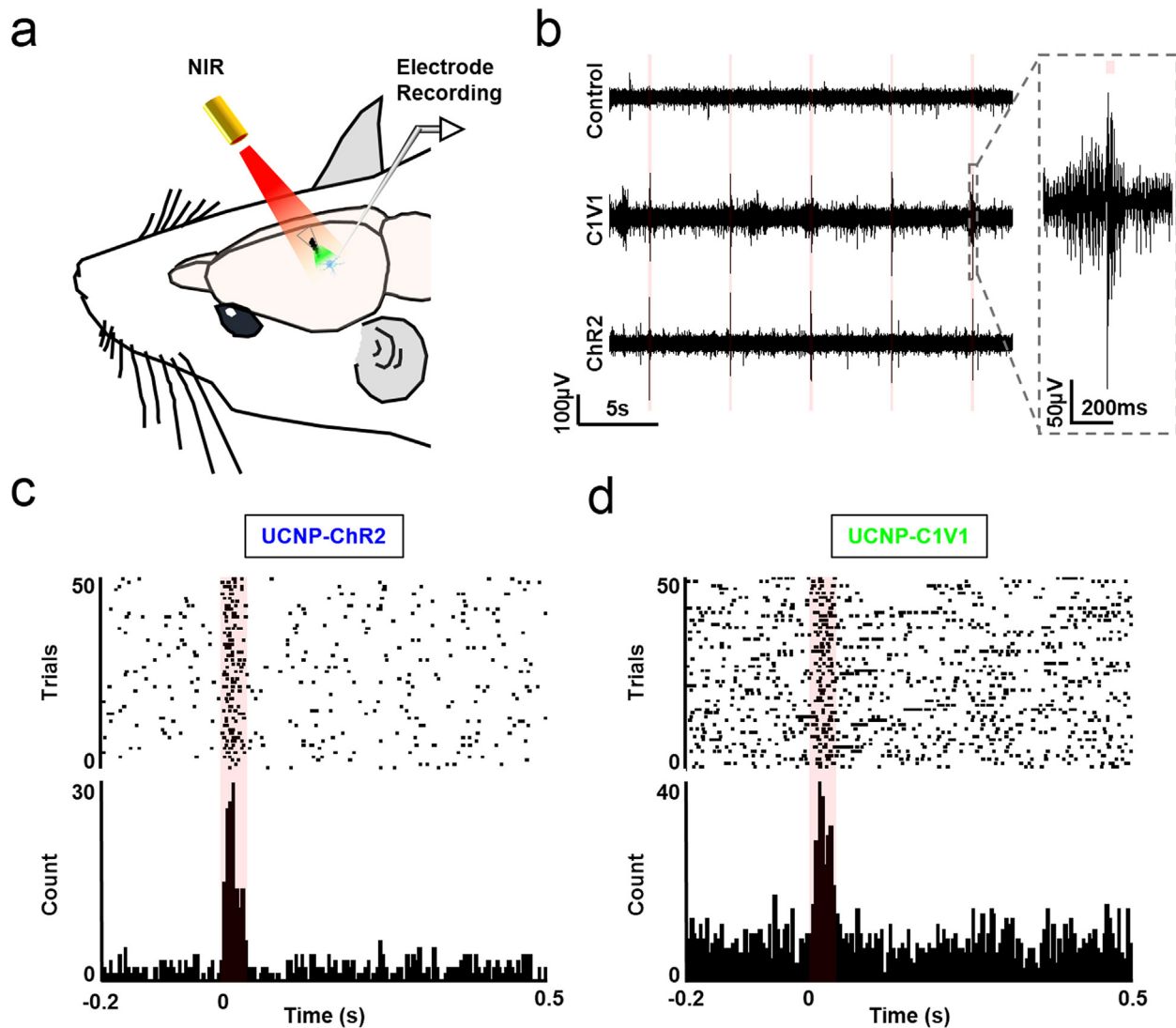


Fig. 4. *In vivo* neural stimulation using an implanted UCNP device. (a) Schematic of the upconversion-based neural stimulation and extracellular recording in brains of anesthetized animals. (b) Representative recordings of NIR-driven spiking traces in animals expressing different ChR variants (ChR2 and C1V1). Radiation from a 980 nm laser was applied at 2 Hz (40 ms pulse width, 4.4 mW/mm² for C1V1 animals and 7 mW/mm² for ChR2 animals). C1V1 animals implanted with a null-optrode (without UCNPs) were used as the control group. (c) Raster plots and peri-stimulus time histograms (PSTHs, 5 ms/bin, 50 trials) showing the temporal correlation between increased spiking activity and NIR illumination in ChR2 animals (40 ms pulse width, 7 mW/mm²). (d) Raster plots and PSTHs (5 ms/bin, 50 trials) showing the temporal correlation between increased spiking activity and NIR illumination in C1V1 animals (40 ms pulse width, 4.4 mW/mm²). In these experiments, five animals were used for each condition.

illumination (Fig. 7g). This rate was significantly higher than those of the animals in the control groups, whose success rates were around or below 40% (Fig. 7h, $p < 0.001$, one-way analysis of variance). Especially for trials requiring a long holding period of 1500 ms, which were the most difficult for the animals due to their limited patience, the success rate in properly stimulated animals was 3-fold higher than it was in wild-type (intact) animals ($57 \pm 4.1\%$ vs. $14 \pm 1.6\%$, mean \pm s.e.m., $n = 4$). Taken together, these results suggest successful modulation of reflexive learning behavior in rats, further exemplifying the power of the upconversion-based tetherless neural stimulation technique.

Supplementary video related to this article can be found at <http://dx.doi.org/10.1016/j.biomaterials.2017.07.017>.

3. Discussion and conclusion

Here we describe an all-optical system for tetherless control of brain activity using upconversion-based implantable micro-

devices. With optogenetics emerging as an important technical advance in neuroscience research, optical intervention has become increasingly popular for selective interrogation of circuit elements in normal and pathological conditions. A typical optogenetic experiment however usually requires the insertion of fiber optics that are tethered to external light sources [11]. This may be a problem for chronic or longitudinal experiments in behaving animals and underscores the need for tether-free brain stimulation strategies. Our approach combines upconversion technology with robotic instrumentation and provides an all-optical solution for flexible tetherless control of brain activity. In our experiments, UCNPs were packaged in glass micro-pipettes to make fully implantable devices, which were used as transducers to convert tissue-penetrating NIR light to higher-energy visible wavelengths matching the activation spectra of commonly used opsin proteins. Traditional optogenetic experiments can thus be performed using remotely applied NIR as the stimulus signal. In contrast to wireless optogenetic strategies utilizing radio-frequency signals to power

implanted LEDs/micro-LEDs [12–15] (Supplementary Table S1), our upconversion-based method does not require any electronic components. Therefore, the fully implantable UCNP-device is extremely small (~100 μm in diameter) and light (less than 1 mg). This is critical in alleviating stress in small animals and helps to reduce surgical lesions resulting from implantation procedures.

Using our method, we demonstrated efficient transcranial neural stimulation at various depths in mouse or rat brains (~4.5 mm at the VTA, ~3 mm at the cortical striatum, and ~1 mm at the visual cortex). We also showed that the stimulation depth can potentially be increased to beyond ~1 cm and span a whole rat brain (Supplementary Movie S1). This kind of deep brain stimulation may be challenging when using alternative optical methods utilizing red-shifted rhodopsins [8,17], such as Chrimson, which is activated by 660 nm light [17] (Supplementary Fig. S5). We found that the superior penetration capability of our technique is achieved in a synergistic manner by combining the advantages of NIR lasers and transparent glass micro-optrodes, which help guide and facilitate the delivery of NIR into deep brain regions (Supplementary Fig. S6). In addition to their transducing functions, which bridge the spectral gap between NIR and VIS, the packaged UCNPs also result in concentrated emission from a tiny spot at the tip of the micro-optrode (~100 μm in diameter) to provide visible light at sufficiently high power densities in close proximity to brain tissue for optogenetic stimulation. Without UCNPs, the same transparent optrode was not able to conduct visible light for neural stimulation if the illumination was applied from outside the brain, suggesting the pivotal role of UCNPs in this novel technique.

Even though upconversion is generally a process with low efficiency, the emission from the UCNP-optrodes (doped with Tm^{3+} or Er^{3+}) was sufficient to effectively activate neurons expressing ChR2 or C1V1. As indicated by fluorescent imaging in live animals, the visible light emitted from UCNP-optrodes could extend as far as two hundred microns. The optrodes thus have a neural activation range of several cell layers, which is a similar distance to that achieved using optical fibers, as indicated by *c-fos* expression after neuronal activation (Supplementary Fig. S7). In addition, the highly tunable optical properties of UCNPs can potentially be tailored to match more ChR variants [30,36,37], further providing potential flexibility for experiments requiring complex activation or silencing patterns. The upconversion process results sequential discrete absorption of two or more lower-energy photons, therefore, NIR-optogenetic control can be achieved using inexpensive and readily available continuous-wave diode lasers. The technique is thus highly cost-effective and simple in its practical implementation. Our upconversion-based tetherless neural stimulation system can be readily set up in other laboratories along with the in-house developed robotic laser projection equipment. With further optimization of different components in the system, such as the packaging of UCNPs, implantation procedures, and laser illumination parameters, etc., the neural stimulation range, effectiveness, and complexity could potentially be further improved. For the first time, this study provides an innovative demonstration of an upconversion-based, all-optical, tetherless brain stimulation strategy in behaving animals. We anticipate that the technique would benefit both basic and translational neuroscience research.

4. Experimental section

4.1. UCNP synthesis and characterization

The nanoparticles were synthesized using a modified procedure involving the growth of $\text{NaYF}_4\text{:Yb/Er}$ core nanoparticles followed by epitaxial coating of NaYF_4 shells [38]. Specifically, in a typical procedure for the synthesis of $\text{NaYF}_4\text{:Yb/Er}$ (or Tm) nanoparticles,

2 ml aqueous solution of $\text{RE}(\text{Ac})_3$ (0.2 M, RE = Y, Yb, Er, or Tm) was added to a 50 ml flask containing 3 ml of oleic acid and 7 ml of 1-octadecene. The mixture was heated at 150 $^\circ\text{C}$ for 30 min before cooling to 50 $^\circ\text{C}$. Shortly thereafter, a methanol solution (5 ml) containing NH_4F (1.6 mmol) and NaOH (1 mmol) was added and the solution was stirred for 30 min. After the methanol was evaporated, the solution was heated to 300 $^\circ\text{C}$ under argon for 1.5 h and then cooled to room temperature. The resulting nanoparticles were precipitated by addition of ethanol, collected by centrifugation, washed with methanol and ethanol several times, and finally redispersed in cyclohexane. To coat the NaYF_4 protection shell, an aqueous solution of $\text{Y}(\text{Ac})_3$ (0.2 M, 2 ml) was mixed with oleic acid (3 ml) and 1-octadecene (7 ml) in a 50 ml flask and subsequently heated at 150 $^\circ\text{C}$ for 30 min before cooling to 50 $^\circ\text{C}$. $\text{NaYF}_4\text{:Yb/Er}$ (or Tm) core nanoparticles in cyclohexane (4 ml) were added along with a methanol solution (5 ml) of NH_4F (1.6 mmol) and NaOH (1 mmol). The resulting mixture was stirred at 50 $^\circ\text{C}$ for 30 min, after which time the solution was heated to 300 $^\circ\text{C}$ under argon for 1.5 h and then cooled to room temperature. The resulting nanoparticles were precipitated by addition of ethanol, collected by centrifugation, washed with methanol and ethanol several times, and redispersed in cyclohexane.

4.2. Animals

Sprague-Dawley (SD) rats and C57BL mice were used in this study. All animal procedures were approved by the university Animal Ethics Committee (Ref: 3A-5-201202). Male SD rats (8–9 weeks, 200–300 g in weight) were used for the electrophysiology recordings and reaction-time task experiments. C57BL mice (6–8 week, 20–25 g in weight) were used in experiments involving deep brain stimulation (cortical striatum and VTA). Animals were randomly assigned to different experimental groups before the surgical procedures. No animals were excluded from analysis and no blinding was performed.

4.3. Sample size and statistics

We chose sample sizes large enough to avoid overlap of the error bars of subsequent data points and to achieve statistically significant evaluations of different experimental conditions, as reflected by *p*-values less than 0.01 using hypothesis test analysis. The reported “*n*” numbers indicate biological replicates. For experiments involving stimulation of cortical striatum (Fig. 5), 4–5 mice were used for each condition. For experiments involving deep brain stimulation of VTA (Fig. 6), five mice were used for each condition. For analysis of NIR-triggered behavioral conditioning in reaction-time tasks (Fig. 7), four rats were used for each condition.

All data used for statistical analysis were checked for distribution normality. For normally distributed data, ANOVAs were used to assess statistical significance among the different experimental conditions. Non-parametric Kruskal-Wallis tests were used when the assumption of normality was not met.

4.4. Fabrication of UCNP-based micro-optrodes

UCNP-containing micro-optrodes were made from borosilicate glass capillaries (1.5 mm outer diameter and 1.0 mm inner diameter). The capillaries were pulled on a micropipette puller (Sutter Instruments, P-2000) to create micro-pipettes with tip sizes around 80 μm , which were used as packaging materials for UCNPs. The nanoparticles dispersed in cyclohexane were front-loaded into the tips of the micro-pipettes using a microinjector with negative holding pressure (Xeneworks, Sutter Instrument), which enabled

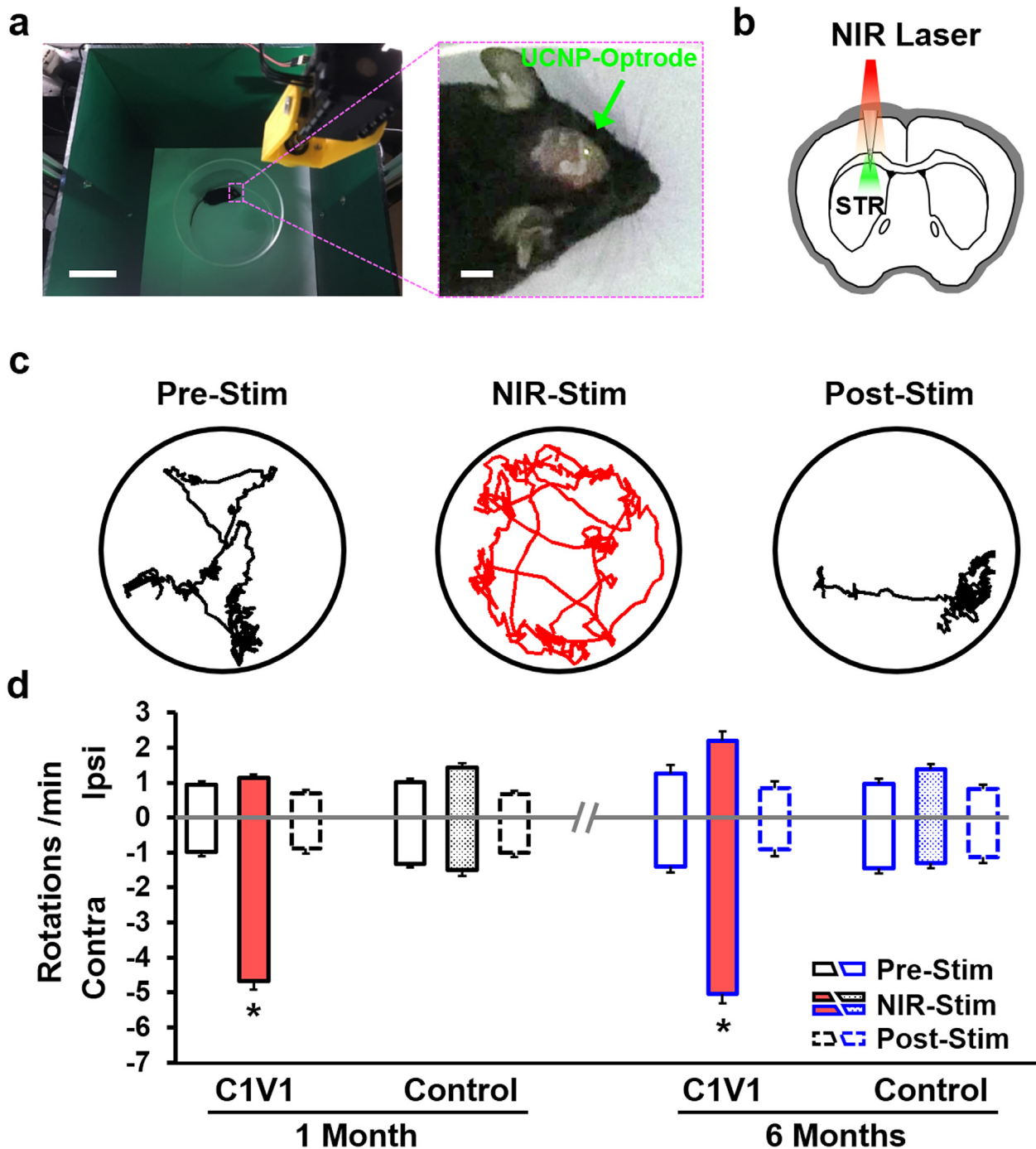


Fig. 5. Tetherless all-optical brain stimulation in behaving animals. (a) Instrumentation of a robotic laser projection system as part of the upconversion-based neural stimulation strategy. Scale bar, 2 cm. The mouse's head is enlarged to show the emission of green light from the implanted UCNP-optrode under NIR irradiation at 5 mW/mm². Scale bar, 5 mm. (b) Schematic of the experimental configuration of unilateral stimulation in the mouse cortical striatum using NIR irradiation. (c) Representative motion-paths from a C1V1 mouse with its cortical striatum activated by the upconversion-based neural stimulation method. (d) Quantitative analysis of rotational movements (contraversive vs. ipsiversive) before (pre-stim.), during (NIR-stim.), and after (post-stim.) NIR illumination. Mice were evaluated one month or six months after surgical implantation of the UCNP-optrode, and subjects with or without C1V1 infection in the striatum were used as test and control groups, respectively. For the one-month experiment, data from 20 sessions were collected from 5 mice. For the six-month experiment, data from 10 sessions were collected from 4 mice. Error bars indicate s.e.m. *p < 0.001 by one way analysis of variance. The NIR laser (20 Hz, 10 ms pulse width, 5 mW/mm²) was consistently applied using a robotic projection system. (For interpretation of the references to colour in this figure legend, the reader is referred to the web version of this article.)

delicate control of loading volume with nano-liter precision. After solvent evaporation, tips of micro-pipettes (filled with dry UCNPs) were sealed using a brief high-temperature treatment. A 3–5-mm segment was then cut from each glass micropipette and the back end was sealed with epoxy to form a UCNP-optrode.

4.5. Virus delivery in animals

The adeno-associated viral (AAV) vectors AAV-CaMKIIa-C1V1(E122T/E162T)-TS-mCherry (serotype 5), AAV-CaMKIIa-hChR2(H134R)-mCherry (serotype 5), and AAV-Syn-ChrimsonR-

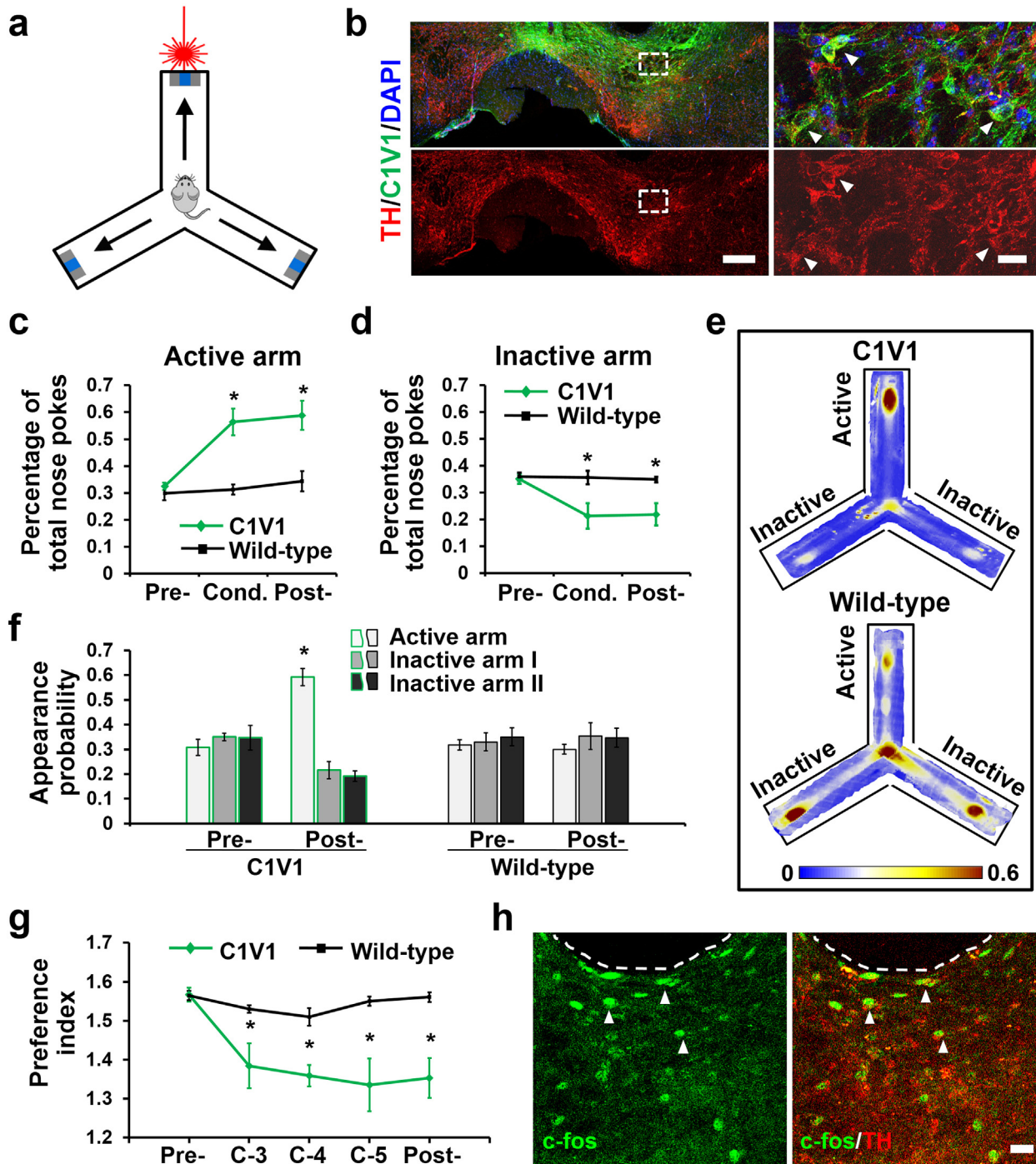


Fig. 6. NIR-conditioned location preference following deep brain stimulation. (a) Schematic of the experiments using a Y-maze. (b) Expression of C1V1 in tyrosine hydroxylase (TH)⁺ dopamine neurons (indicated by arrowheads) in the ventral tegmental area of the mouse brain 3 weeks after injection of adeno-associated viruses. For clarity, the fluorescence images of the boxed regions are enlarged in the right panels. Scale bars: 200 μm (left panels) or 20 μm (right panels). (c) Quantification of the percentage of total nose-pokes in the “Active” arm of a Y-maze over a one-hour period. Each poke in the “Active” arm was paired with a pulsed 980 nm laser (500 ms, 20 Hz, 10 ms pulse width, 5 mW/mm²) (n = 5, error bars indicate s.e.m., *p < 0.01 by one way analysis of variance [ANOVA]). (d) Quantification of the percentage of total nose-pokes in an “Inactive” arm of the Y-maze over the one-hour period (n = 5, error bars indicate s.e.m., *p < 0.01 by one way ANOVA). (e) Heat map showing mouse activity frequency in the post-condition session. Red color represents more frequent appearance in specific parts of the Y-maze. (f) Quantification of the appearance probability before and after the NIR conditioning sessions (n = 5, error bars indicate s.e.m., *p < 0.01 by one way ANOVA). Higher probabilities clearly demonstrate the development of location preference in C1V1 mice. (g) The temporal curve of the animals’ preference indices during the different experimental stages. A decrease in the index reflects an increase in the predictability of the animal’s movement (n = 5 mice, error bars indicate s.e.m., *p < 0.01 by one way ANOVA). (h) Fluorescence images of a horizontal section of mouse brain showing the activation of c-fos in TH⁺ dopamine neurons (indicated by arrowheads) surrounding the UCNP-optrode (outlined) after repeated NIR irradiation for 1 h (5 mW/mm², 10 ms pulse width, 20 Hz, 10 pulses were applied at the beginning of every minute). Scale bar, 20 μm . (For interpretation of the references to colour in this figure legend, the reader is referred to the web version of this article.)

tdTomato (serotype 2) were acquired from the Vector Core at the University of North Carolina at Chapel Hill. Animals (rats/mice)

were anesthetized with sodium pentobarbital (50 mg/kg). Anesthesia was maintained throughout the surgical operations. Fifteen

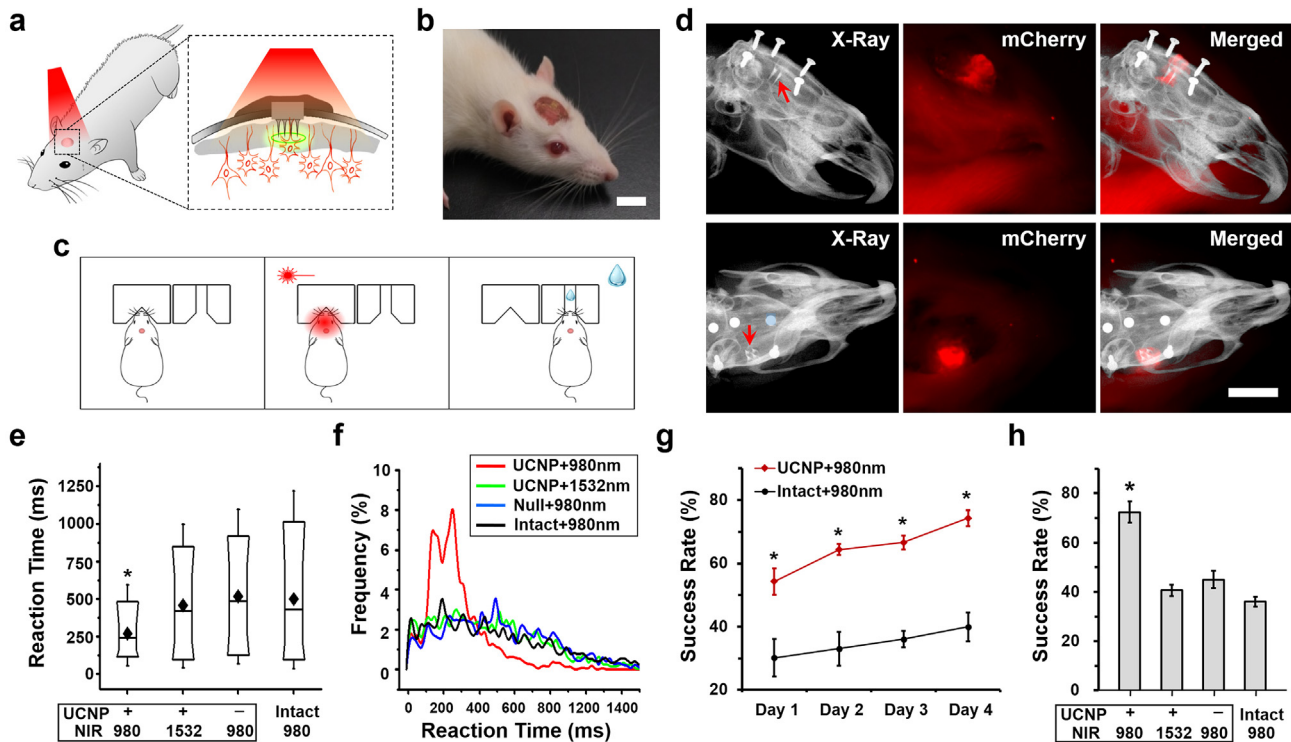


Fig. 7. Implantation of multiple UCNP-optrodes for modulation of reflexive learning in rats. (a) Schematic of surgical implantation of multiple UCNP-optrodes. (b) Photograph of a rat after implantation. Scale bar, 1 cm. (c) Reaction-time tasks using NIR-induced cortical activation as a cue. Trials were initiated upon pokes into the left port. After a random holding period, a 980 nm laser (10 pulses, 10 Hz, 50 ms width, 1.5 mW/mm²) was used to stimulate the animal's visual cortex. This stimulation then cued the animal to move to the right port for a water reward. (d) X-Ray and fluorescence images (top row, lateral view; bottom row, dorsal view) showing the colocalization of micro-optrode implants and ChR2 expression regions. The micro-optrodes are indicated by red arrows in the X-Ray images. Scale bar, 1 cm. (e) Box-plots show the quantification of the animals' reaction times in response to NIR cues. The different parts of the box-plots indicate 10th, 25th, 50th, 75th, and 90th percentiles, while the whiskers indicate the 5th and 95th percentiles. The diamond indicates the mean of the data. **p* < 0.001 by Kruskal-Wallis analysis. (f) Histogram of reaction times for the experimental and control groups. (g) Success rates of animals performing the reaction-time tasks in the first 4 days (*n* = 4, error bars indicate s.e.m., **p* < 0.001 by ANOVA). (h) Success rates for animals after training for 4 days (*n* = 4, error bars indicate s.e.m., **p* < 0.001 by ANOVA). For panels (e–h), the conditions include the use of UCNP-optrodes illuminated by 980 nm or 1532 nm lasers, null-optrodes illuminated by a 980 nm laser, and intact animals illuminated by a 980 nm laser. At least 1000 trials were performed in 4 rats for each condition. (For interpretation of the references to colour in this figure legend, the reader is referred to the web version of this article.)

minutes before the induction of anesthesia, atropine sulfate (0.05 mg/kg) was administered to inhibit tracheal secretions. The animals were then mounted on a stereotactic device for further operation.

For rats, a midline incision was made in the scalp after the liberal application of local anesthetics (xylocaine, 2%). A craniotomy was performed at a location 4.5–6.5 mm posterior and 3.0–5.0 mm lateral to the bregma to access the visual cortex, and the dura mater was removed. Viruses were injected at two locations with the following coordinates: 5.0/6.0 mm posterior, 4.0 mm lateral, and 1.0 mm ventral to bregma. Injections were made using a cannula connected to a syringe pump at a rate of 0.1 μl/min (total volume, 1 μl). After the injection, the cannula was withdrawn, and the injection sites were cleaned with sterile saline and topped with silicone sealant (Kwik-cast, World Precision Instruments). The skin was then sutured back in place, and the rats were left to recover. During the procedures, the body temperatures of the rats were maintained at 37–38 °C using a heating blanket. After 3 weeks, the rats were prepared for further experiments.

For mice, after making an incision on the scalp following application of local anesthetics (xylocaine, 2%), a hole (0.6 mm diameter) was made on the skull at the appropriate location using an electric dental drill to access brain tissue. To infect the VTA, 0.5 μl of AAV viruses were injected into the brain at the following coordinate: 3.44 mm posterior, 0.48 mm lateral, and 4.4 mm ventral to bregma. To infect the cortical striatum, 0.5 μl of AAV viruses were

injected into the brain tissue at the following coordinate: 1.1 mm posterior, 1.7 mm lateral, and 3 mm ventral to bregma. Injections were made at a rate of 0.02 μl/min (total volume, 0.5 μl) using a glass micro-pipette connected to a syringe pump. After withdrawing the injection micropipette, the injection sites were cleaned with sterile saline, and the skin was sutured. During the procedures, the body temperatures of the mice were maintained at 37–38 °C using a heating blanket. The mice were used for further experiments three weeks later.

4.6. UCNP-optrode implantation

Implantation of UCNP-based micro-optrodes was performed 3 weeks after virus injection using a stereotactic apparatus (Supplementary Fig. S1b–k). During the surgical operations, the animals were anesthetized as described above, and a similar craniotomy was performed. The silicone sealant was removed before implanting any devices.

For acute *in vivo* electrophysiology experiments, bundles combining a UCNP-optrode and a tungsten electrode were inserted into the virus injection sites (5.0–6.0 mm posterior, 4.0 mm lateral, and 1.0 mm ventral to bregma). Electrical measurements were performed in anesthetized animals immediately afterwards. For behavioral experiment in rats, four UCNP-optrodes were inserted into tissues around the injection sites (5.0–6.0 mm posterior, 3.5–4.5 mm lateral, and 1.0 mm ventral to bregma). For behavioral

experiments in mice, a single UCNP-optrode was inserted into the appropriate brain region at the virus injection site. For cortical striatum stimulation, the stereotactic coordinates were 1.1 mm posterior, 1.7 mm lateral, and 3 mm ventral to bregma. For VTA stimulation, the stereotactic coordinates were 3.44 mm posterior, 0.48 mm lateral, and 4.5 mm ventral to bregma. All animals were allowed to recover for at least one week before proceeding to behavioral experiments.

4.7. Behavioral study in rats using reaction-time tasks

Behavioral studies in freely moving animals were performed at least one week after all surgical operations. After the recovery period, animals with significant weight loss were excluded from the experiments. The subjects were trained in a two-port operant chamber to characterize their response to remote NIR stimulation. In this task, an animal, which was previously maintained using a restricted water supply, was first habituated in the chamber for familiarization with the nose-poke and water-seeking tasks for one day. It was then trained to poke into the left port (waiting hole) to initiate a trial and required to stand still for a random waiting period (800, 1000, 1200 or 1500 ms) before the application of sequences of 10 NIR pulses (980 nm, 50-ms pulse width, 1.5 mW/mm²) from an overhead light source. This stimulation then cued the animals to obtain water rewards from the right port (rewarding hole). The reaction times and success rates were used as major parameters to access the subject's performance. Though the water reward was presented in the rewarding hole for 2 s after each NIR cue, only trials with reaction times longer than 100 ms and shorter than 600 ms were considered successful NIR-stimulated trials.

4.8. NIR-conditioned location-preference in mice

NIR stimulation of the VTA was performed in mice to condition their location preference [14]. Briefly, C1V1-infected mice (with implanted UCNP-optrodes) were prepared for experiments by mildly restricting their water supply to facilitate behavioral responses. Mice were then placed in an unbiased Y-maze with three compartments (Supplementary Fig. S3). Each arm of the Y-maze was 30 cm long and 5 cm wide, and was connected by a triangular region (total area of 460 cm²). Homemade nose-poke devices were installed at the distal ends of the arms and the numbers of nose-poke by the mice were automatically recorded using a commercial system (Tucker-Davis Technologies).

The mouse was first placed in the Y-maze and allowed to freely explore the entire apparatus for one day (pre-conditioning) in order to familiarize itself to the environment. From day 2 to day 3 (conditioning phase I), the animal was further allowed to explore the Y-maze. During this time, a nose-poke in the “Active” arm was paired with a 500-ms 980 nm illumination (10 ms pulse width, 20 Hz, 5 mW/mm²), which was used to stimulate the VTA in the mouse brain. The conditioning was completed daily until 300 nose-pokes were achieved. From day 4 to day 6 (conditioning phase II), the mice were allowed to explore the Y-maze for one hour each day, and their behaviors were recorded by a camera. Nose-pokes were still paired with NIR illumination in the “Active” arm (Supplementary Movie S4). After the conditioning period, the animals were allowed to rest for one day. From day 8 to day 9 (post-conditioning), NIR illumination was removed from the system and the mouse was placed in the Y-maze for one hour each day. The behaviors of the mice were recorded on camera for later analysis.

To analyze the animal's behavior in the Y-maze, the recorded one-hour-long video was first sampled at 1 Hz to produce a stack of time-course images. The whole stack was then averaged at every pixel to derive a background reference, which was subtracted from

the raw images to extract the “mouse signal”. The location of the mouse at a specific time point was determined using the “mouse signal”. Summing up all “mouse signals” from all images resulted in a map of mouse activity, wherein areas of higher appearance frequency were colored in red, and those of lower frequency were colored in yellow. A template of the Y-maze was used to filter out noise signals outside of the mouse movement areas. Information entropy of mouse appearance probability in each of the three arms was used as an indicator of the predictability of mouse movement (preference index), which reflects the animal's location preference following conditioning by NIR stimulation of the VTA deep in the mouse brain. The information entropy $H(X)$ was calculated as:

$$H(X) = - \sum_{i=1}^3 P(x_i) \log_2 P(x_i)$$

given that $X \in \{x_1, x_2, x_3\}$ and $P(x_i)$ were the probability of mouse appearance within Arm_{*i*} of the Y-maze.

4.9. Robotic laser projection system and stimulation of cortical striatum

To accommodate flexible and consistent brain stimulation using the upconversion-based technique, a robotic laser projection system was developed for automatic tracing of the mouse head. This system was used to place a single NIR illumination spot on the mouse's head in real-time. In this system, two rotational motors (AX-18A, Dynamixel) and a 3D-printed holding beam were assembled to form a robotic arm, which was placed ~50 cm above the animal. This arm was used to project NIR illumination at arbitrary coordinates in a 40 × 40 cm experimental field. A high-speed camera was installed beside the robotic arm for video recording. Before the experiments, the coordinates of the experimental field (40 × 40 cm) were digitized and mapped with a resolution of 0.25 mm (0.29°) using a calibration scan. Movement of the robotic arm was achieved using a custom-developed program in Python, which was used for the automatic identification of the targeting spot on the animal's head. The image processing procedures included the following 6 steps (Supplementary Fig. S2): 1) every frame from the video recording was processed in real-time; 2) a region of interest was defined; 3) the color space was transformed from RGB to HSV; 4) a binary mask was generated using the HSV image; 5) blob detection was used to identify large features on the animal's head; 6) after removing the noise blobs, the average coordinates of the largest three blobs were taken as the target position and then sent to the control board for laser projection.

For stimulation of the mouse cortical striatum, a cylinder 30 cm in diameter was placed in the laser projection system for better visualization. Mice were placed in the cylinder and allowed to behave freely. A testing cycle consisted of three one-minute sessions: pre-stimulation, stimulation, and post-stimulation. NIR illumination was applied only during the stimulation session using the robotic projection system (10 ms pulse width, 20 Hz, 5 mW/mm²). The animal's movements and turning behavior were then quantitatively analyzed based on the recorded movie.

4.10. Immunohistochemistry

To perform immunohistochemistry, rats/mice were anesthetized with pentobarbital and transcardially perfused with 0.9% NaCl and 4% paraformaldehyde. Brains were extracted and fixed for at least 1 day at 4 °C. Samples were then bathed in 30% sucrose solution (diluted in phosphate-buffered saline [PBS]) until the brain tissue settled to the bottom. The brains were then cut into 50-μm-

thick slices by frozen sectioning (Cryostar NX70, Thermo Scientific) and mounted on glass slides. All brain slices were thoroughly rinsed with PBS and blocked in 4% bovine serum albumin in Tris-buffered saline containing 0.25% Triton X-100 overnight at 4 °C. The slices were then incubated with primary antibodies overnight at 4 °C and rinsed thoroughly with Tris-buffered saline before incubation with secondary antibodies for 1 h at room temperature. The stained brain slices were then rinsed with PBS and mounted on glass slides for imaging. Samples were imaged using a confocal scanning laser microscope equipped with a 40× water immersion objective (TCS SP8, Leica Microsystems). The primary antibodies used in this study included rabbit anti-c-fos (Abcam, ab190289, 1:2000 dilution), rabbit anti-GFAP (Millipore, AB5804, 1:1000 dilution) goat anti-Iba1 (Abcam, ab5076, 1:500), and sheep anti-tyrosine hydroxylase (Abcam, ab113, 1:500).

4.11. Live animal imaging

In vivo imaging of live animals was carried out using a multi-model imaging system (In-Vivo Xtreme, Bruker). The rats/mice were anesthetized by injection of sodium pentobarbital (50 mg/kg). Both X-ray and fluorescence images were acquired. A 600 nm emission filter (35 nm band-pass window) was used for mCherry. In order to excite UCNP-optrodes, a 980 nm laser system was custom-installed within the animal imager and illumination was applied from above. A 535 nm emission filter (35 nm band-pass window) was used for UCNPs emitting green light.

Acknowledgment

This work was supported by General Research Funds from RGC Hong Kong SAR (GRF11278616, GRF11218015, and GRF11211314), a Health and Medical Research Fund from the Food and Health Bureau of Hong Kong SAR (HMRP 03141146), and by Collaborative Research Funds from RGC Hong Kong SAR (C5015-15G, C1014-15G). This work is also partially supported by General Research Funds awarded to M.L. (GRF21202816 and GRF16212815).

Appendix A. Supplementary data

Supplementary data related to this article can be found at <http://dx.doi.org/10.1016/j.biomaterials.2017.07.017>.

Author contributions

P.S. conceived the project, designed and supervised the experiments, and wrote the manuscript. Y.W., X.L., Z.X., and W.Z. performed the experiments and analyzed the data. C.C. and F.W. synthesized and characterized the nanoparticles. X.C. and J.H. helped with the animal experiments and provided constructive discussions. X.D. and X.W. performed analysis of the video recordings of animal behavior. W.Z., Q.L., and M.L. implemented the robotic laser projection system.

Competing financial interests

The authors declare no competing financial interests.

References

- [1] M.R. Warden, J.A. Cardin, K. Deisseroth, Optical neural interfaces, *Annu. Rev. Biomed. Eng.* 16 (2014) 103–129.
- [2] O. Yizhar, L.E. Fenno, T.J. Davidson, M. Mogri, K. Deisseroth, Optogenetics in neural systems, *Neuron* 71 (2011) 9–34.
- [3] G. Nagel, T. Szellas, W. Huhn, S. Kateriya, N. Adeishvili, P. Berthold, et al., Channelrhodopsin-2, a directly light-gated cation-selective membrane channel, *Proc. Natl. Acad. Sci. U. S. A.* 100 (2003) 13940–13945.
- [4] E.S. Boyden, F. Zhang, E. Bamberg, G. Nagel, K. Deisseroth, Millisecond-timescale, genetically targeted optical control of neural activity, *Nat. Neurosci.* 8 (2005) 1263–1268.
- [5] V. Gradinaru, K.R. Thompson, K. Deisseroth, eNpHR: a Natronomonas halorhodopsin enhanced for optogenetic applications, *Brain Cell Biol.* 36 (2008) 129–139.
- [6] F. Zhang, M. Prigge, F. Beyriere, S.P. Tsunoda, J. Mattis, O. Yizhar, et al., Red-shifted optogenetic excitation: a tool for fast neural control derived from *Volvox carterii*, *Nat. Neurosci.* 11 (2008) 631–633.
- [7] J. Mattis, K.M. Tye, E.A. Ferenczi, C. Ramakrishnan, D.J. O’Shea, R. Prakash, et al., Principles for applying optogenetic tools derived from direct comparative analysis of microbial opsins, *Nat. Methods* 9 (2012) 159–172.
- [8] J.Y. Lin, P.M. Knutsen, A. Muller, D. Kleinfeld, R.Y. Tsien, ReaChR: a red-shifted variant of channelrhodopsin enables deep transcranial optogenetic excitation, *Nat. Neurosci.* 16 (2013) 1499–1508.
- [9] A. Berndt, S.Y. Lee, C. Ramakrishnan, K. Deisseroth, Structure-guided transformation of channelrhodopsin into a light-activated chloride channel, *Science* 344 (2014) 420–424.
- [10] B.J. Tromberg, N. Shah, R. Lanning, A. Cerussi, J. Espinoza, T. Pham, et al., Non-invasive *in vivo* characterization of breast tumors using photon migration spectroscopy, *Neoplasia* 2 (2000) 26–40.
- [11] F. Zhang, V. Gradinaru, A.R. Adamantidis, R. Durand, R.D. Airan, L. de Lecea, et al., Optogenetic interrogation of neural circuits: technology for probing mammalian brain structures, *Nat. Protoc.* 5 (2010) 439–456.
- [12] K.L. Montgomery, A.J. Yeh, J.S. Ho, V. Tsao, S. Mohan Iyer, L. Grosenick, et al., Wirelessly powered, fully internal optogenetics for brain, spinal and peripheral circuits in mice, *Nat. Methods* 12 (2015) 969–974.
- [13] C.T. Wentz, J.G. Bernstein, P. Monahan, A. Guerra, A. Rodriguez, E.S. Boyden, A wirelessly powered and controlled device for optical neural control of freely-behaving animals, *J. Neural Eng.* 8 (2011) 046021.
- [14] T.I. Kim, J.G. McCall, Y.H. Jung, X. Huang, E.R. Siuda, Y. Li, et al., Injectable, cellular-scale optoelectronics with applications for wireless optogenetics, *Science* 340 (2013) 211–216.
- [15] S.I. Park, D.S. Brenner, G. Shin, C.D. Morgan, B.A. Copits, H.U. Chung, et al., Soft, stretchable, fully implantable miniaturized optoelectronic systems for wireless optogenetics, *Nat. Biotechnol.* 33 (2015) 1280–1286.
- [16] J.V. Frangioni, *In vivo* near-infrared fluorescence imaging, *Curr. Opin. Chem. Biol.* 7 (2003) 626–634.
- [17] N.C. Klapoetke, Y. Murata, S.S. Kim, S.R. Pulver, A. Birdsey-Benson, Y.K. Cho, et al., Independent optical excitation of distinct neural populations, *Nat. Methods* 11 (2014) 338, 972.
- [18] J.P. Rickgauer, D.W. Tank, Two-photon excitation of channelrhodopsin-2 at saturation, *Proc. Natl. Acad. Sci. U. S. A.* 106 (2009) 15025–15030.
- [19] A.M. Packer, D.S. Peterka, J.J. Hirtz, R. Prakash, K. Deisseroth, R. Yuste, Two-photon optogenetics of dendritic spines and neural circuits, *Nat. Methods* 9 (2012) 1202–1205.
- [20] R. Prakash, O. Yizhar, B. Grewe, C. Ramakrishnan, N. Wang, I. Goshen, et al., Two-photon optogenetic toolbox for fast inhibition, excitation and bistable modulation, *Nat. Methods* 9 (2012) 1171–1179.
- [21] E. Papagiakoumou, A. Begue, B. Leshem, O. Schwartz, B.M. Stell, J. Bradley, et al., Functional patterned multiphoton excitation deep inside scattering tissue, *Nat. Phot.* 7 (2013) 274–278.
- [22] W. Denk, J.H. Strickler, W.W. Webb, 2-Photon laser scanning fluorescence microscopy, *Science* 248 (1990) 73–76.
- [23] A.M. Packer, B. Roska, M. Hausser, Targeting neurons and photons for optogenetics, *Nat. Neurosci.* 16 (2013) 805–815.
- [24] F. Auzel, Upconversion and anti-stokes processes with f and d ions in solids, *Chem. Rev.* 104 (2004) 139–173.
- [25] C. Wang, L.A. Cheng, Z.A. Liu, Drug delivery with upconversion nanoparticles for multi-functional targeted cancer cell imaging and therapy, *Biomaterials* 32 (2011) 1110–1120.
- [26] N.M. Idris, Z.Q. Li, L. Ye, E.K.W. Sim, R. Mahendran, P.C.L. Ho, et al., Tracking transplanted cells in live animal using upconversion fluorescent nanoparticles, *Biomaterials* 30 (2009) 5104–5113.
- [27] N.M. Idris, M.K. Gnanasammandhan, J. Zhang, P.C. Ho, R. Mahendran, Y. Zhang, *In vivo* photodynamic therapy using upconversion nanoparticles as remote-controlled nanotransducers, *Nat. Med.* 18 (2012) 1580–1585.
- [28] X. Wu, Y. Zhang, K. Takle, O. Bilsel, Z. Li, H. Lee, et al., Dye-sensitized core/active shell upconversion nanoparticles for optogenetics and bioimaging applications, *ACS Nano* 10 (2016) 1060–1066.
- [29] S. Hososhima, H. Yuasa, T. Ishizuka, M.R. Hoque, T. Yamashita, A. Yamanaka, et al., Near-infrared (NIR) up-conversion optogenetics, *Sci. Rep.* 5 (2015) 16533.
- [30] F. Wang, R.R. Deng, J. Wang, Q.X. Wang, Y. Han, H.M. Zhu, et al., Tuning upconversion through energy migration in core-shell nanoparticles, *Nat. Mater.* 10 (2011) 968–973.
- [31] J.L. Wu, F.C. Chen, M.K. Chuang, K.S. Tan, Near-infrared laser-driven polymer photovoltaic devices and their biomedical applications, *Energ Environ. Sci.* 4 (2011) 3374–3378.
- [32] A.V. Kravitz, B.S. Freeze, P.R. Parker, K. Kay, M.T. Thwin, K. Deisseroth, et al., Regulation of parkinsonian motor behaviours by optogenetic control of basal ganglia circuitry, *Nature* 466 (2010) 622–626.
- [33] F. Tecuapetla, S. Matias, G.P. Dugue, Z.F. Mainen, R.M. Costa, Balanced activity in basal ganglia projection pathways is critical for contraversive movements, *Nat. Commun.* 5 (2014) 4315.

- [34] H.C. Tsai, F. Zhang, A. Adamantidis, G.D. Stuber, A. Bonci, L. de Lecea, et al., Phasic firing in dopaminergic neurons is sufficient for behavioral conditioning, *Science* 324 (2009) 1080–1084.
- [35] Y. Imai, S. Kohsaka, Intracellular signaling in M-CSF-induced microglia activation: role of Iba1, *Glia* 40 (2002) 164–174.
- [36] J.C. Boyer, C.J. Carling, B.D. Gates, N.R. Branda, Two-way photoswitching using one type of near-infrared light, upconverting nanoparticles, and changing only the light intensity, *J. Am. Chem. Soc.* 132 (2010) 15766–15772.
- [37] X. Chen, D. Peng, Q. Ju, F. Wang, Photon upconversion in core-shell nanoparticles, *Chem. Soc. Rev.* 44 (2015) 1318–1330.
- [38] F. Wang, R.R. Deng, X.G. Liu, Preparation of core-shell NaGdF₄ nanoparticles doped with luminescent lanthanide ions to be used as upconversion-based probes, *Nat. Protoc.* 9 (2014) 1634–1644.